Chapter 2

2.1 Introduction

Bismuth ferrite ($BiFeO_3$) abbreviated as BFO, is the most promising lead-free material among other multifunctional ceramics because of its ferroelectric and ferromagnetic coupling above room temperature. The bulk BFO has a rhombohedral structure with R*3c* space group, and the super-exchange interactions between two magnetically active Fe^{3+} and non-magnetic O^{2-} ions (Fe^{3+}-O^{2-}-Fe^{3+}) (*i.e.*, transfer of an electron between partially filled and vacant orbital) give rise to G–type antiferromagnetic ordering. In BFO, coupling between one magnetic ion and one non-magnetic ion leads to a generally ferromagnetic character. So, various substitutions (A-site, B-site, and co-substitution at A and B-site) have been done on BFO to improve the ferromagnetic, and ferroelectric properties substitution alters one electron bandwidth, which depends on the alteration of Fe^{3+}-O^{2-}-Fe^{3+} bond angle.

2.2 Structure of BFO

$BiFeO_3$ has a perovskite structure in which both the cations, Bi and Fe, are trivalent. The Bi^{3+} ions (A-site) are present in a simple cubic arrangement such that each $BiFeO_3$ unit cell consists of two such cubes sharing a corner along the [111] direction (Fig. 1.16). The Fe^{3+} ions (B-site) are coordinated with six O^{2-} ions, and each of the two Bi^{3+} cubes contain one FeO_6 octahedra. However, the FeO_6 octahedra are tilted along the $[001]_{hex}$ axis, distorting the $BiFeO_3$ unit cell to produce a rhombohedral structure.

For the structural stability of BFO, ionic radii should be matched well according to the Goldschmidt tolerance factor '*t*' defined according to equation 1.1. Ideally, the tolerance factor should be nearly 1, but for BFO, it is 0.89 [Catalan *et al.* 2009]. Smaller tolerance factors

(produced by the substitution with a smaller cation) imply shrinkage of the cells formed by Bi^{3+} ions, which cause increased buckling and tilting of the FeO_6 octahedra, causing a reduction Fe-O-Fe bond angle from 180° to 154°-156°. The Fe–O–Fe angle controls both the magnetic exchange and orbital overlap between Fe^{3+} and O^{2-} ions, i.e., it determines the magnetic properties and electrical conduction. However, if the substituted cation is too small, it creates an unstable structure as it transforms toward the hexagonal arrangement. Therefore, the tolerance factor should not reduce below 0.86. The list of substituents given at A-site and B- sites in BFO is shown in Fig. 2.1 with the help of periodic table.

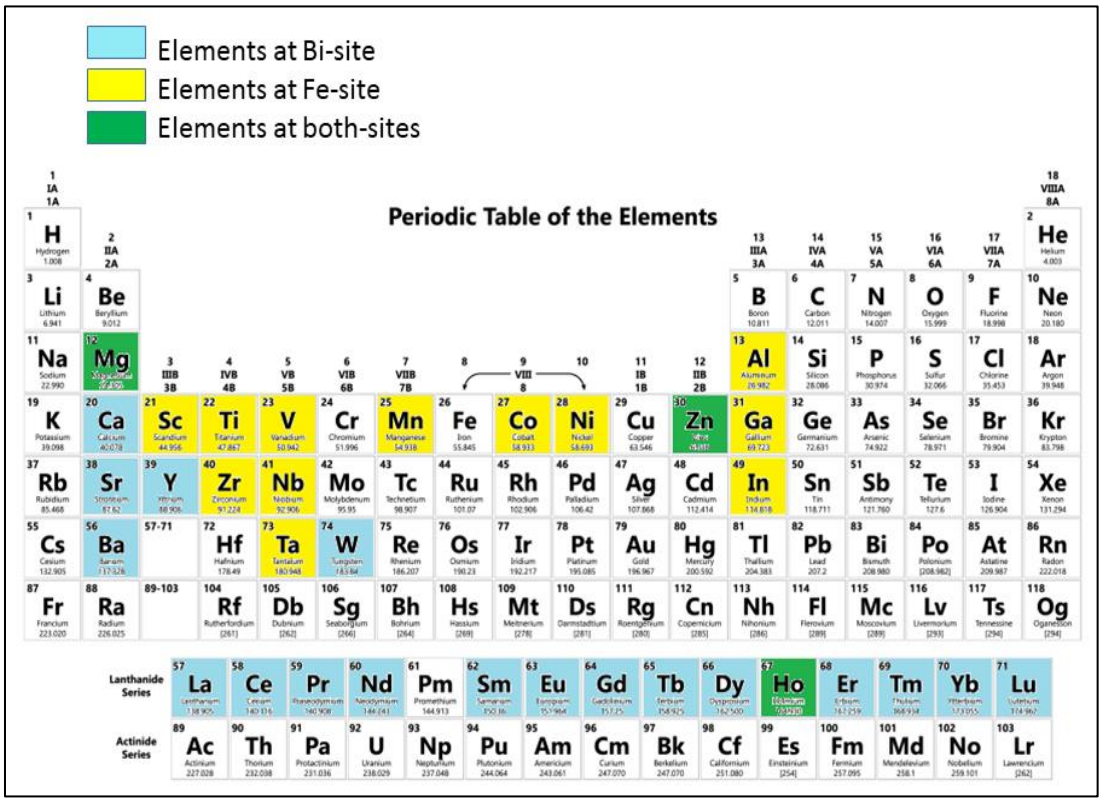

Fig. 2.1 Different substituents are shown in the periodic table; elements in blue color boxes show doping at Bi-site, elements in yellow color boxes show doping at Fe-site, and elements in green color boxes may be doped at Bi and Fe-site both.

2.3 Doping of elements at Bi-site

Doping of rare earth (RE) ions at the bismuth site play an essential role in improving the physical properties. The REs has partially filled *f*-shells which are spatially located closer to the core region, protected by the outer shells of stable 5*s* and 5*p* orbitals. Therefore, rare-earth ions are inert; they don't make a strong bond with neighboring oxygen ions. It occupies the vacant spaces between the oxygen octahedra and controls the bond angle that indirectly affects the physical properties. The doping at the A-site by divalent cations like Ca^{2+} and Sr^{2+} may realize novel conducting states of hole-doped $BiFeO_3$ unless other dopants like oxygen vacancies are produced. Because of charge neutrality, some of the ligand levels in the valence band may be vacant, *i.e.*, hole carriers are introduced by control of band filling. On the other hand, doping with Ce^{4+} ions are known to produce electron carriers. Different rare earth elements, *i.e.*, Y, La, Ce, Pr, Nd, Sm, Eu, Gd, Tb, Dy, Ho, Er, Tm, Yb, Lu, are doped in BFO. The ionic radii with CN=8, are taken from database provided by Shannon [Shannon 2019]. Table 2.1 summarizes different dopants at Bi-site in BFO systems.

Table 2.1 List of elements doped at Bi-site in BFO.

Name of element	Atomic no.	Electronic configuration	Ionic radius [Å]
Bismuth (Bi)	**83**	**[Xe] $4f^{14}5d^{10}6s^26p^3$**	**1.17**
Yttrium (Y)	39	[Kr] $4d^1\ 5s^2$	0.8
Lanthanum (La)	57	[Xe] $5d^1\ 6s^2$	1.16
Cerium (Ce)	58	[Xe] $5d^14f^16s^2$	1.18
Praseodymium (Pr)	59	[Xe] $4f^3\ 6s^2$	1.12
Neodymium (Nd)	60	[Xe] $4f^46s^2$	1.109

Samarium (Sm)	62	[Xe] $4f^6 6s^2$	1.079
Europium (Eu)	63	[Xe] $4f^7 6s^2$	1.066
Gadolinium (Gd)	64	[Xe] $4f^7 5d^1 6s^2$	1.053
Terbium (Tb)	65	[Xe] $4f^9 6s^2$	1.04
Dysprosium (Dy)	66	[Xe] $4f^{10} 6s^2$	1.027
Holmium (Ho)	67	[Xe] $4f^{11} 6s^2$	1.015
Erbium (Er)	68	[Xe] $4f^{12} 6s^2$	1.004
Thulium (TI)	69	[Xe] $4f^{13} 6s^2$	0.994
Ytterbium (Yb)	70	[Xe] $4f^{14} 6s^2$	0.985
Lutetium (Lu)	71	[Xe] $4f^{14} 5d^1 6s^2$	0.977
Scandium (Sc)	21	[Ar] $3d^1 4s^2$	0.87
Cadmium (Cd)	48	[Kr] $4d^{10} 5s^2$	1.1
Strontium (Sr)	38	[Kr] $5s^2$	1.26
Barium (Ba)	56	[Xe] $6s^2$	1.42
Calcium (Ca)	20	[Ar] $4s^2$	1.12
Magnesium (Mg)	12	[Ne] $3s^2$	0.89

2.3.1 Doping of RE elements at Bi-site in BFO

Bellakki *et al.* in 2009, compared the properties of $BiFeO_3$ and $Bi_{0.98}Y_{0.02}FeO_3$ ceramics prepared using the solution combustion route. The enhanced magnetic properties are found. In 2011, Hou *et al*. have prepared $BiFeO_3$ and $Bi_{0.95}Y_{0.05}FeO_3$ using the hydrothermal route under similar conditions. It is observed that the magnetic properties are significantly enhanced at room

temperature, achieved saturation magnetization of 2.3 emu/g. Microwave dielectric properties of $Bi_{0.95}Y_{0.05}FeO_3$ nano-crystals are analyzed in the range of 2-18 GHz. The Y doping increases permeability, enhancing the spin relaxation of domain wall motion and weakening electron-relaxation caused by decreasing Fe^{2+}, respectively.

La^{3+} and Bi^{3+} have almost equal ionic radii. La doping decreases the bismuth vacancy. La based samples of $Bi_{1-x}La_xFeO_3$ (x = 0, 0.08, 0.15, 0.30) are prepared using polymeric precursor method (Pechini method). A structural phase transition from rhombohedral to orthorhombic is observed near x = 0.30 [Garcia *et al.* 2010]. Suresh *et al.* in 2013 have composed $La_xBi_{1-x}FeO_3$ (x = 0.0-0.4) ceramics by the solid-state reaction method. It is found to be a decrement in rhombohedral (~92.4% to ~58.39%) and an increment in the orthorhombic phase (~7.59% to ~41.60%). The samples have shown spin-glass behavior, and the T_N increased with the doping concentration.

Ce^{3+} and Bi^{3+} have similar ionic radii, so it is easy to control the Bi volatilization by stabilizing the oxygen octahedral [Sharma *et al.* 2017]. Cerium has two valence states, Ce^{3+} and Ce^{4+}, that could control the reduction of Fe^{3+} to Fe^{2+}. Hybridization takes place between the $4f^1$ electron of the Ce^{3+} ion and empty $5d^0$ and $6s^0$ orbitals of the Ce^{3+} ion, as well as the $2p^6$ electrons of the O^{2-} ion. Meanwhile, the $5p^6$ electrons of the Ce^{4+} ion make contact with empty $4f^0$, $5d^0$, and $6s^0$ orbitals of the Ce^{4+} ion as well as the $2p^6$ electrons of the O^{2-}ion [Pradhan *et al.* 2012]. In 2012, Pradhan *et al.* have synthesized $Bi_{1+x}Ce_xFeO_3$ (x =0.0, 0.05, 0.1, 0.15) monophasic ceramic samples using conventional solid-state reaction routes. It is found that the electrical conductivity is decreased, and dielectric behavior is improved. The oxygen vacancies get reduced, resulting in huge suppression of leakage current.

In 2019, Arti *et al.* have prepared multiferroic samples of $Bi_{1-x}Pr_xFeO_3$ (x =0.0, 0.05, 0.10, 0.15, 0.20) ceramics using sol-gel method. It is observed that the dielectric and magnetic properties were improved. For x =0.15, the bandgap of 2.27 eV was observed. Madolappa *et al.* 2016 have synthesized $Bi_{1-x}Pr_xFeO_3$ (x =0.0, 0.05, 0.1) nano-powder samples via sol-gel route. It is found that the grain and grain boundary resistances were decreases with the increasing temperature. The temperature-dependent frequency plots of dielectric, modulus, and impedance show the "non-monodispersive Debye process" and reflect the influence of grain and grain boundaries.

Wang *et al.* in 2015 have composed $Bi_{1-x}Nd_xFeO_3$ (x=0.00, 0.05, 0.075, 0.10) ceramic samples. It is found that the dielectric and magnetic properties increase and oxygen vacancies decrease with doping. The nano-crystals of $Bi_{1-x}Nd_xFeO_3$ (x= 0.00, 0.05, 0.1, 0.15) were prepared by solution combustion technique. It is revealed that the Nd substitution transformed the rhombohedral to triclinic phase that reduces the impurities. It is also found that with increasing Nd concentration average grain size reduces from 74 to 26 nm while remanent magnetisation increases [Gautam *et al.* 2011].

Liu *et al.* in 2009 have prepared $Bi_{1-x}Eu_xFeO_3$ (x=0.0, 0.10, 0.15) nanoparticles synthesized with sol-gel route. The M_r is found around 0.13 emu/g, which is relatively higher than other non-magnetically rare earth elements (Nd^{3+}, La^{3+}, Sm^{3+}) doped BFO. The solubility limit is observed at x =10% of BFO. $Bi_{0.85}Eu_{0.15}FeO_3$ samples have been prepared through solid-state reaction by Reddy *et al.* 2009. Spontaneous magnetization is observed due to weak ferromagnetism of the Dzyaloshinskii–Moriya type. Uniyal *et al.* in 2009 have prepared $Bi_{1-x}Eu_xFeO_3$ (x= 0.03,0.05,0.07,0.1) ceramic samples by convention -al solid-state reaction technique. An improved dielectric, electric, and magnetic properties are observed with Eu

doping. The highest value of remnant polarization and remnant magnetization is obtained for x=0.1, and the values of P_r and M_r are 11 μC/cm^2 and 0.0347 emu/g, respectively.

The ionic radii of Gd^{3+} (107.8Å) are smaller than Bi^{3+} (1.17Å) and possess a high magnetic moment (μ_B =7.9 BM) [Iorguet *et al.* 2015]. Guo *et al.* in 2010 have composed $Bi_{1-x}Gd_xFeO_3$ (x =0.0, 0.05, 0.1, 0.15) nanoparticles prepared by a sol-gel derived route. An enhanced magnetic and dielectric properties are found due to the distorted spin cycloid and the ferromagnetic coupling between Gd^{3+} and Fe^{3+} ions. The $Bi_{1+2x}Gd_{2x/2}Fe_{1-2x}O_3$ (x= 0, 0.05, 0.1, 0.15) ceramics are prepared by solid-state route by Pradhan *et al.* 2011. The leakage current density for the x = 0.15 sample is 0.3×10^{-6} A/mm^2, which is about four orders of magnitude lower than pure BFO. The saturation polarization value is obtained at around 15 μC/cm^2.

Tb^{3+} has a high magnetic moment among all the lanthanides, *i.e.*, 9.33μ/μ_B. So, it is expected to enhance the magnetization and suppress the spiral spin structure of BFO with the doping content. Chen *et al.* in 2010 have fabricated $Bi_{1-x}Tb_xFeO_3$ (x = 0.05 – 0.16) thin films via a metal-organic deposition method on indium tin oxide/glass substrates. At x = 0.11 it is found a maximum saturated magnetization and piezoelectric coefficient values M_s = 22.2 emu/cm^3 and d_{33} =140 pm/V, respectively. The nanoparticles of $Bi_{1-x}Tb_xFeO_3$ (x= 0, 0.01, 0.03 and 0.05) were prepared by the sol-gel technique. It is noticed that for all the Tb doped samples have rhombohedral structure. Tb^{3+} substitution reduces the particle size and increases the ferromagnetic properties. At room temperature huge remanent magnetization value of 1.73 emu/g was obtained for x=0.01. Also, the leakage current density was improved for all the samples [Guo *et al.* 2014].

Dy^{3+} has the highest magnetic moment (10.55 μ/μ_B) among lanthanides. In 2014, Sati *et al.* have fabricated $Bi_{1-x}Dy_xFeO_3$ (x =0.0, 0.03, 0.05, 0.07, 0.10, 0.12) ceramic samples by solid-state reaction route. It is observed a maximum remnant magnetization at x = 0.12 with a value of 0.2103 emu/g. The optical band gap is obtained in the visible region. The polycrystalline sample of $Bi_{0.9}Dy_{0.1}FeO_3$ ceramic is synthesized by a solid-state reaction. The ferroelectric and ferromagnetic properties are improved, and the value M_r is obtained at around 0.118 [Chowdhury *et al.* 2017].

Suresh *et al.* in 2014 have composed $Ho_xBi_{1-x}FeO_3$ (x = 0.00, 0.10, 0.15, 0.20) ceramics using solid state reaction method. It is observed a highest M_r = 17.9 emu/g value for x = 0.2 composition at room temperature. Polycrystalline $Bi_{1-x}Ho_xFeO_3$ (x = 0.0, 0.05, 0.10, 0.15, 0.20) samples are composed by the conventional solid-state route. Electrical and magnetic properties are improved for x = 0.15 composition and the observed values are $2P_r$ = 16 $\mu C/cm^2$ and $2M_r$ = 0.1256 emu/g, respectively [Pradhan *et al.* 2010].

$Bi_{1-x}Er_xFeO_3$ (x =0.00, 0.10, 0.15) nanoparticles are prepared by using the sol-gel route. The M_r is obtained at around 0.428, which is the highest among all the A-site dopants. An increasing permittivity and decreasing leakage current are also noticed [Zhou *et al.* 2013]. In 2021, Sharma *et al.* have prepared $Bi_{1-x}Er_xFeO_3$ (x =0.0, 0.04, 0.08, 0.12) nanoparticles using sol-gel route. A pure rhombohedral is stable up to x = 0.08; then, the orthorhombic phase dominates. Ferroelectric properties are enhanced, and the optical band energy ranges from 2.10 eV to 1.70 eV.

In 2019, Auromun *et al.* have prepared Tm-doped $Bi_{1-x}Tm_xFeO_3$ (x =0.0 and 0.15) compound using the conventional high-temperature solid-state reaction route. It is revealed that

the dielectric constant and ferroelectric properties increase, whereas the dielectric losses do not improve. Kuz *et al.* 2013 have composed $Bi_{1-x}R_xFeO_3$ (R =Er, Tm, Yb) ceramics. They have varied x within the range of 0.05-0.25 for Er and Yb and 0.0-0.12 for Tm. The partial substitution of Er and Tm in $BiFeO_3$ reduces the temperature of the ferroelectric phase transition *R3c–Pbnm* at 30-60 K. $Bi_{1-x}Lu_xFeO_3$ (x =0.00, 0.02, and 0.04) samples are synthesized using the solid-state reaction method. It is found that the remanent magnetization rises up to x =0.02, and the obtained value is 3.3×10^{-3} kOe [Morales-Rivera *et al.* 2020]. Yan *et al.* 2007 have prepared $Bi_{1-x}Yb_xFeO_3$ (x =0.0, 0.05, 0.10, 0.15, 0.2) ceramic samples using rapid liquid phase sintering. The smallest leakage current is obtained with 15% Yb doped $BiFeO_3$. The current density with $<10^{-7}$ A/cm^2 and the largest remnant polarization around 8.5 μ/cm^2 is found with doping.

2.3.2 Doping of non-RE elements at Bi-site in BFO

The substitution of divalent ions in trivalent (Bi^{3+}) cause the charge imbalance that originates three possibilities *viz.*, (i) oxidation of Fe^{3+} into Fe^{4+}, (ii) formation of oxygen vacancies, and (iii) co-occurrence of two or more crystal phases [Brahmi *et al.* 2016 and 2017]. These competing phenomena give rise to interesting physical properties.

Sarkar *et al.* in 2016 have synthesized $Bi_{1-x}Sc_xFeO_3$ (x =0.0, 0.05, 0.10, 0.15, 0.20, 0.25) nano-particulates and nano-fibres using conventional sol-gel method and electrospinning, respectively. It is revealed that the band gap decreases, and the magnetic properties enhanced with increasing concentration of Sc. Fibres have better properties than particulates, such as magnetic saturation and catalytic stability are better.

Bellakki *et al.* in 2010 have fabricated $Bi_{1-x}Cd_xFeO_3$ (x =0.0, 0.05, and 0.1) ceramic samples by a citrate-gel method. The highest value of remanent magnetization (0.96 emu/g) is

obtained for 10% Cd in $BiFeO_3$ samples. Ishaq *et al.* in 2016, prepared the nanoparticles of $Bi_{0.75}Cd_{0.25}Fe_{1-x}Mn_xO_3$ (x =0.0, 0.05, 0.10, 0.15) using micro-emulsion technique. They found with increasing Mn concentration the dielectric properties decreases while magnetic properties improved.

Polycrystalline samples of $Bi_{1-x}Sr_xFeO_3$ (x =0.00, 0.05, 0.10, 0.20, and 0.30) ceramics are prepared by sol-gel auto-combustion route. The maximum values of remanence magnetization and coercivity are obtained for x =0.30 and the values are 0.175 emu/g and 366.64 Oe, respectively. The dielectric properties are improved up to 200 °C [Hussain *et al.* 2013]. The nanoparticles of $Bi_{1-x}Sr_xFeO_3$ (x =0.0, 0.15) were synthesized by using sol gel route. It is revealed that with Sr doping the grain size reduces while the oxygen vacancies enhance the magnetic properties and the dielectric properties depreciated [Dhir *et al.* 2018].

Das *et al.* in 2012 have synthesized $Bi_{1-x}Ba_xFeO_3$ (x =0.0, 0.1, 0.15, 0.2, and 0.25) samples using the chemical route. A maximum magnetic moment is found for 15% Ba at room temperature. The maximum fatigue resistance and magnetoelectric coupling are observed for x = 0.20. The nano-particle samples of $Bi_{1-x}Ba_xFeO_3$ (x =0, 0.05, 0.10, 0.15, and 0.20) are synthesized using the molten salt route. It is observed that the particle sizes and oxygen vacancies are decreased with Ba doping. The leakage current densities decrease by one order of magnitude. The dielectric and magnetic properties of the nanoparticles are also improved [Wu *et al.* 2019].

In 2018, Xian *et al.* have prepared nanoparticles of $Bi_{1-x}Ca_xFeO_3$ ($0 \leq x \leq 0.25$) ceramics using the sol-gel route. The oxygen vacancies and M_r are increased with increasing Ca concentration. The value of magnetization is 0.096 emu/g obtained at x = 0.10. $Bi_{1-x}Ca_xFeO_3$ (x

=0.00, 0.05, 0.10, 0.15, 0.20) thin films are prepared by sol-gel process. The grain sizes decrease, and band gap increases with increasing Ca concentration [Yao *et al.* 2017].

Mishra *et al.* in 2017 have prepared the polycrystalline ceramic samples of $Bi_{1-x}Mg_xFeO_3$ (x =0.0, 0.1, 0.15, 0.2) by solid-state method. The ferroelectric properties and bandgap are improved for Mg-doped samples. The nano crystallites of $Bi_{1-x}Mg_xFeO_3$ (x =0.0, 0.02, 0.04) were composed using sol-gel route. It is observed that magnetic and ferroelectric properties increase [Li *et al.* 2016].

It can be concluded that the doping at Bi-site may significantly enhance the ferroelectric and piezoelectric properties of the BFO system, primarily due to structural and phase changes associated with the A-site doping.

2.4 Doping of elements at Fe-site

Fe-site is usually doped with the cations of other elements of large mismatch to create oxygen vacancies or oxidize the iron. Mostly 3*d*-transition metals are doped at Fe-site to band formation, while chemical bonding between Fe^{3+} and O^{2-} ions controls the electronic conduction. B-site doping plays an essential role in controlling the physical properties by changing the electronic structure near the Fermi level. The impurities are located at random sites as a point defect in these elements. Some of these impurities create midgap states that control the material's optical and conduction properties [Yang *et al.* 2012].

2.4.1 Doping of non-RE elements at Fe-site in BFO

Polycrystalline samples of $BiFe_{1-x}Sc_xO_3$ (x =0, 0.05, 0.1 and 0.15) are prepared using solid-state reaction method. The AC conductivity decreases with Sc doping due to the decrease in oxygen vacancies and Fe^{2+} ions in BFO [Rao *et al.* 2014].

Wang *et al.* 2006 have synthesized thin films of $BiFe_{1-x}Ti_xO_3$ (x =0.05, 0.1, 0.15) ceramics by sol-gel spin-coating technique. A large enhancement in both remnant and saturation polarization is revealed with the Ti-doped-$BiFeO_3$. The saturation magnetization and saturation polarization values are M_s ~20 emu/cm^3 and P_s ~32 μC/cm^2, respectively. Bernardo 2013 has prepared ceramic samples of $BiFeO_3$ and $BiFe_{0.95}Ti_{0.05}O_3$ compounds using a mixed-oxide route. It is revealed that the direct-current resistivity is increased, and the compound is ferromagnetic, with the highest coercive field value of 27 kOe at 4K temperature.

Chauhan *et al.* 2012 have prepared nanoparticles of $BiFe_{(1-x)}Mn_{(x)}O_3$ (x = 5, 10, and 15 mol%) ceramics using sol–gel technique. The saturation magnetisation of 0.33 emu/g is found for 15 mol % Mn doping. The magnetoelectric coupling is improved up to 2.5% with 15 mol % doping. $BiFe_{1-x}Mn_xO_3$, (x =0.0, 0.1, 0.2) nanoparticles are synthesized by modified sol-gel processing technique. Magnetisation and dielectric properties are enhanced with Mn doping up to x = 0.02 [Sharma *et al.* 2019].

Xu *et al.* 2009 have synthesized $Bi(Fe_{0.95}Co_{0.05})O_3$ bulk ceramics by rapid sintering using the sol-gel route. The spin-glass behavior and meta-magnetism are observed. $BiFe_{1-x}Co_xO_3$ (x = 0.00, 0.01, 0.03 and 0.05) nanoparticles are synthesized by the sol-gel technique. It is noticed that the dielectric constant increases and dielectric loss decreases. Overall, enhanced ferromagnetic properties are obtained with Co substitution.

$BiFe_{1-x}Ni_xO_3$ ($0 \leq x \leq 0.5$) samples are synthesized by the solid-state route. For x = 0.1, the maximum value of specific magnetization (M_s) of 2.9 emu/g is obtained. It is revealed that for $x \geq 0.4$, the rhombohedral phase is transformed to $NiFe_2O_4$, and the associated ferromagnetic order (M_s = 9.2 emu/g) is enhanced. The sintered powders of $x \leq 0.1$ exhibit ε_r ~1000 and tanδ

~0.3 at 100 kHz[Betancourt-Cantera *et al.* 2018]. Kumar *et al.* 2011 have prepared the nanoceramic samples of $BiFe_{1-x}Ni_xO_3$ (x = 0, 0.1) using the sol-gel method. The samples show spin-glass behavior. The magnetization and dielectric constant for quenched samples are 3.04 emu/g at 10 kOe and 930, respectively.

The nanoparticles of $BiFe_{1-x}Zn_xO_3$ (x = 0, 0.05, 0.1, 0.2, and 0.3) are synthesized by a modified sol-gel route, and thin films are fabricated on $LaNiO_3$ buffered surface oxidized Si substrates using pulsed laser deposition technique. It is observed that film with 5% doping of Zn shows better ferroelectricity, grain size, and magnetization [Sheng *et al.* 2013]. Yang *et al.* 2018 have prepared nanoparticles $BiFe_{1-x}Zn_xO_3$ (BFZO) (x = 0.00, 0.01, 0.02, 0.03) via the sol-gel method and fabricated thin films are deposited on ITO/glass substrates. For x = 0.02, a large remnant polarization ($2P_r$ = 129.6 μC/cm^2) and low coercive field ($2E_c$ = 904 kV/cm) at an electric field value of 1000 kV/cm are observed. Under a high electric field, the leakage conduction mechanism transforms from the Ohmic conduction to the F-N tunneling effect.

Mukherjee *et al.* 2010 have synthesized a thin film of $BiFe_{1-x}Zr_xO_3$ (x = 0.0-0.15) by chemical solution deposition on Pt/Si substrates. For the prepared samples, impurity phases are not observed. Also, the dielectric behavior improved, and remanent magnetization is depressed, whereas the relaxation is not shown at low frequencies. Polycrystalline Zr-doped $BiFeO_3$ thin films are prepared by a sol-gel spin-coating technique on (111) $Pt/Ti/SiO_2/Si$ substrates. The prepared film exhibits a weak magnetization with M_s of ~25 emu/cm^3 [Wang *et al.* 2007].

The polycrystalline ceramic samples of Nb-doped $BiFeO_3$ are composed of a solid-state reaction. The room temperature dielectric constant is ε=100, and unsaturated electrical hysteresis loops are obtained. The samples have shown ferromagnetic-like behavior with M_r = 0.015 emu/g

and H_c = 500 Oe [Jun *et al.* 2005]. The thin films of $BiFe_{1-x}Nb_xO_3$ (x = 0, 0.3, 1, 3) are epitaxially grown on $SrRuO_3$-buffered $SrTiO_3$ substrates. The polarization loops are shifted horizontal and indicate an effective internal electric field [Zhou *et al.* 2019]. The solid solution of $Bi_{0.8}Na_{0.2}Fe_{0.8}Nb_{0.2}O_3$ is prepared by a solid-state route. It is noticed that the sample show non-Debye type relaxation behavior [De *et al.* 2018].

Nanoparticles of $BiFe_{1-x}Mg_xO_3$ (x =0.0, 00.05, 0.1) are synthesized by co-precipitation route. The samples exhibit ε′ from 10^3-10^5 over the temperature range of 200−473 K [Kum-onsa *et al.* 2020]. Xu *et al.* in 2015 have prepared $BiFe_{0.5}Mn_{0.5}O_3$ films and $BiFeO_3/BiMnO_3$ superlattices using pulsed laser deposition on (001) $SrTiO_3$ substrates. It is observed that both the samples show spin-glass behavior, and the thermo-remanent magnetization is decreased with time. These samples are found antiferromagnetic in nature.

The ceramics powders of $BiFe_{1-m}Al_mO_3$ (*m* =0, 2%, 4%, 6% and 8%) are synthesized by sol-gel method. The coercive field ($2E_c$), resistivity, and residual polarization intensity ($2P_r$ and ΔP) of 4% ceramic are recorded as 43.7 kV/cm, 3.71 × 10^6 Ω·m, 1.93, and 1.28 μC/$cm^{2,}$ respectively. The leakage currents of the substituted ceramics are decreased by 2-3 orders of magnitude and are dominated by Ohmic and space-charge-limited conduction [Cao *et al.* 2020]. Chandel *et al.* 2017 have synthesized ceramic samples of $BiAl_xFe_{1-x}O_3$ (x = 0.0, 0.025, 0.05, 0.075, 0.1) by citrate precursor method. The magnetic properties deteriorate, but the leakage current is highly decreased. The dielectric constant is noticed around 51 at 100 kHzfor x = 0.1.

It is concluded that doping at the B-site successfully improves both the leakage current behavior and magnetism without disturbing the ferroelectric and piezoelectric performances in the BFO system.

2.4.2 Doping of RE elements at Fe-site in BFO

Xu *et al.* in 2009 have prepared the nano-powders of $BiFe_{1-x}Ta_xO_3$ (x = 0, 0.05, 0.1) synthesized by sol-gel method. The M_s value is obtained at around ~0.05 μB/Fe. Microwave dielectric spectra reveal a damped resonant response. Polycrystalline ceramic samples of $BiFe_{1-x}Ta_xO_{3+x}$ (x = 0, 0.01, 0.02, 0.03) are composed by a solid-state reaction. It is found that the electrical resistivity of doped samples increases by six orders of magnitude as compared to pure BFO. The samples also show intrinsic coupling between the magnetic and electric dipole at RT [Jun *et al.* 2007].

2.5 Doping of ABO_3 systems in BFO

There are many monophase multiferroic BFO compounds have been studied but problems such as huge leakage current; structural instability and distortion; and low magnetoelectric coupling are still unresolved. So, an attempt to solve these problems, perovskite systems like have been doped $BaTiO_3$, $NaNbO_3$, $SrTiO_3$, $PbTiO_3$, $CaTiO_3$ [Choudhary *et al.* 2007].

Ji *et al.* 2021 have prepared the ceramic samples of (1-*x*) $BiFeO_3$-*x*$BaTiO_3$ (*x* = 0.2, 0.25, 0.3, 0.35, 0.4) by solid-state reaction with microwave sintering and conventional sintering methods. It is found that up to x = 0.3, single-phase (*R3c*) is obtained, but for x ≤ 0.35 $Pm\bar{3}m$, the structure is observed. It is revealed that CS method is better than MWS as the dielectric and ferroelectric properties get reduced by microwave sintering. For x = 0.35 the value of P_r is 3.74 μC/cm^2 and 2.22 μC/cm^2 for CS and MWS, respectively.

Saad *et al.* 2018 have prepared the electroceramic samples of (x)$NaNbO_3$–(1-x) $BiFeO_3$ (x = 0.15, 0.25, 0.50, 0.75, 0.85, 1). The PTCR behavior is reported above room temperature for 0.5≤x ≥1, and the obtained T_{max} values are 410 K, 393 K, 405 K, and 463 K, respectively.

The solid solutions of $BiFeO_3$-$SrTiO_3$ (BFO-STO) are prepared by a conventional solid-state route. Core-shell structure is found in all the doped samples. It is noticed that the samples in the range of $0.7 \geq x \geq 0.575$ exhibits high remanent polarization (30-50 μC cm^{-2}). The maximum d_{33} value of 69 pCN^{-1} is obtained for x = 0.625, which is 75% higher than undoped BFO (~ 40 pCN^{-1}) [Makarovic *et al.* 2019].

Botero *et al.* 2011 have prepared the $0.6BiFeO_3$–$0.4PbTiO_3$ samples by using a high-energy ball-milling process. The piezoelectric coefficients, *i.e.*, $d_{31} = -41.6\times10^{-12}$ m/V and $g_{31} = -9.65\times10^{-3}$ Vm/N (at RT) ae obtained. It has three times higher piezoelectric coefficients than previous reports for synthesized piezoceramics through the conventional route.

The nanoparticles of $0.8BiFeO_3$–$0.2CaTiO_3$ are preapred by the sol-gel route. The synthesized powders were heat-treated at different temperatures 500 °C, 650 °C, 800 °C, and 950 °C. The magnetization is enhanced, but the samples show spin-glass behavior.

Choudhary *et al.* in 2007, prepared solid solution of (1-x) $BiFeO_3$ – (x) $BaZr_{0.4}Ti_{0.6}O_3$ [BFO-BZT] (x =0.00, 0.15, 0.25, 0.40, 0.50) using solid-state reaction techniques. They revealed the dielectric properties were deteriorated while leakage current improved.

So overall, it can be concluded that the doping of ABO_3 type systems enhances both the piezoelectric and magnetic performances compared to the undoped system.

In this study we have fixed 10% Sm at Bi site of $BiFeO_3$ in order to enhance the properties of pure BFO. So, for this study the general formula of base composition is $Bi_{0.9}Sm_{0.1}FeO_3$. The detailed explanation for 10% Sm fixation is described further in section 2.6.

2.6 Effect of Sm substitution

Rare-earth ions are smaller than Bi^{3+}. Their doping at the A-site reduces the tolerance factor, decreasing the Fe–O–Fe bond angle, leading to a more electrically insulating character. For instance, Sm^{3+} has smaller ionic radii (1.132Å) than Bi^{3+} (1.365Å), which reduces the tolerance factor from 0.890 for $BiFeO_3$ to 0.887 for $Bi_{0.9}Sm_{0.1}FeO_3$ (BSFO) [Catalan *et al.* 2004]. Their unit cell parameters are shown in Table 2.2. The normalized unit cell parameters are calculated using Equation (2.1).

$$a_{norm} = \left(\frac{1}{\sqrt{2}}\right) a_{hex} \text{ and } c_{norm} = \left(\frac{1}{\sqrt{2}}\right) c_{hex} \quad (2.1)$$

Table 2.2 Effect of Sm doping on hexagonal and normalized unit cell parameters of $BiFeO_3$.

Composition	a_{hex}(Å)	c_{hex}(Å)	a_{norm}(Å)	c_{norm}(Å)
$BiFeO_3$	5.578	13.868	3.944	4.003
$Bi_{0.9}Sm_{0.1}FeO_3$	5.566	13.797	3.936	3.983

Thus, It can be seen that $\frac{a_{hex\,(Bi_{0.9}Sm_{0.1}FeO_3)}}{a_{hex}(BiFeO_3)}$ = 99.8% and $\frac{c_{hex\,(Bi_{0.9}Sm_{0.1}FeO_3)}}{c_{hex}\,(BiFeO_3)}$ = 99.5%, which implies that doping of Sm in Bi reduces the tetragonality of the system. The normalization approaching unity means a more cubic and stable crystal structure. The absence of lone pairs in Sm^{3+} cation makes the tetragonal polar structure weak. A phase transition occurs upon 15 mol% Sm^{3+} ion substitution. Sm has partially filled *f*-shells which are spatially located closer to the core region and are protected by outer shells of stable 5*s* and 5*p* orbitals. The Sm^{3+} ions do not form a strong chemical bond with neighboring O^{2-} ions while occupying the empty spaces between oxygen octahedra (FeO_6) which indirectly controls the Fe-O-Fe bond angle and band

filling by donating electrons to the B-site ions [Yang *et al.* 2012]. Table 2.3 summarizes the dielectric and magnetic properties of BSFO compared to BFO systems synthesized through different routes. By investigating the above results shown in Table 2.3, it can be concluded that the doping of Sm at the Bi within the BFO system up to a fixed level of 0.1 provide an overall enhancement of dielectric constant, remanent magnetization, and remanent polarization values along with lowering the dielectric losses.

Table 2.3. Comparison of dielectric and magnetic properties of BSFO systems synthesized through different routes

Comp.	Route	ε′	tan δ	M_r	P_r	Ref.
BFO	Solid state route	–	–	–	–	Khomchenko *et al.* 2014
BSFO		–	–	0.15emu/g	–	
BFO	Solid-state route	–	–	~0 emu/g	–	Maurya *et al.* 2009
BSFO		–	–	$\sim 3\times10^{-3}$ emu/g	–	
BFO	Thin-film by PLD	–	–	–	–	Cheng *et al.* 2010
BSFO		–	–	–	~100 μC/cm^2	
BFO	Solid-state route	–	–	$\sim 3.17\times10^{-4}$ emu/g	~0.30 μC/cm^2	Nalwa *et al.* 2008
BSFO		–	–	$\sim 2.2\times10^{-2}$ emu/g	~0.60 μC/cm^2	
BFO	Sol-gel route	–	–	–	–	Schiemer *et al.* 2012
BSFO		@ RT at 10kHz ε'~100	@ RT at 10kHz ~0.23	at 300 K 0.0277emu/g	=20 μC/cm^2	

BFO	Sol-gel route	–	–	–	–	Puli *et al.* 2012
BSFO		375K at 1kHz ε =210	375K at 1kHz ~0.017	At 300K 4×10^{-4} emu/g	–	
BFO	Sol-gel route	–	–	~0.0 emu/g	~3 $\mu C/cm^2$	Mukherjee *et al.* 2015
BSFO		–	–	~0.3 emu/g	~7 $\mu C/cm^2$	
BFO	Thin film by spin coater	–	–	$\sim1.5\times10^{-3}$ emu/cm^3	–	Anthonyraj *et al.* 2015
BSFO		–	–	$\sim 2\times10^{-2}$ emu/cm^3	–	
BFO	Solid state route	–	–	–	–	Palaimiene *et al.* 2015
BSFO		$\sim10^4$ at 1.21 kHz	–	–	–	
BFO	Rapid liquid phase sintering	–	–	$=1.8\times10^{-3}$ emu/g	–	Singh *et al.* 2015
BSFO		–	–	$=6.14\times10^{-2}$ emu/g	–	
BFO	Pyrolysis-crystallization	@ RT at 10 kHz ε'~148	@ RT at 10 kHz ~0.042	–	At 5kHz ~ 80 $\mu C/cm^2$	Sun *et al.* 2015
BSFO		ε'~152	~0.055		~60 $\mu C/cm^2$	
BFO	Solid phase synthesis	@ 500k ε' ~ 100	–	–	–	Kallaev *et al.* 2016
BSFO		ε' ~100	–	–	–	
BFO	Co-precipitation method	@RT at 1kHz ε'= 1.1×10^4	@RT At 1kHz ~0.5	–	–	Yotburut *et al.* 2017
BSFO		ε' ~ 10^4	~ 0.6	–	–	

BFO	Sol-gel synthesis	At 373K, $\Delta\varepsilon = 11.06\times10^3$	At 473K ≥10	0 emu/g	–	Deka *et al.* 2017
BSFO		At 373K, $\Delta\varepsilon = 3.27\times10^3$	At 473K ≥1	0.1 emu/g	–	
BFO	Mechano-synthesis	–	–	–	–	Gonzalez *et al.* 2017
BSFO		at 425K ε_r = 950 at 100kHz	–	0.031emu/g	–	
BFO	Sol–gel based electrospinning process	–	–	0.02 emu/g	–	Yan *et al.* 2018
BSFO		@RT at 10kHz ε ~ 22	@RT at 10kHz ~ 0.2	0.075emu/g for nanoparticles	–	
BFO	Sol-gel route	@ RT at 100kHz, ε'=38.66	@ RT at 100kHz 0.0393	=0.151emu/g	@50Hz =0.211 μC/cm^2	Singh *et al.* 2019
BSFO		ε'=53.02	0.0239	=0.488 emu/g	=0.575 μC/cm^2	
BFO	Sol-gel route	@RT at 10kHz ε'~16	@RT at 10kHz ~0.042	= 67 emu/g = 1.16 emu/g	at 20kV/cm = 0.057 μC/cm^2	Rhaman *et al.* 2019
BSFO		ε'~28	~0.027	–	=0.068 μC/cm^2	
BFO	Sol-gel route	at 300 °C, ε' ~ 2.5×10^2	–	–	–	Sadykov *et al.* 2019
BSFO		ε' ~ 5×10^2	–	–	–	
BFO	Sol-gel route	at 10.8 GHz ε'=3.7616	at 10.8 GHz 0.088526	–	–	Goldab *et al.* 2020
BSFO		ε'=3.5395	0.079814	–	–	
BFO	Solid state route	ε'=68	–	1.81×10^{-3} emu/g	–	Ain *et al.* 2012

BSFO		ε'=70	–	1.84×10^{-2} emu/g	–	
BFO	Solid state route	–	–	–	–	Khomchenko *et al.* 2010
BSFO		–	–	~0.1 emu/g	–	

2.7 Outcome of literature review

We have summarized the research carried out on BFO multiferroic in bulk, thin films, composites sample prepared with different processing methods like conventional solid state reaction method, rapid phase/microwave sintering and sol-gel combustion route. Many other studies excluded in this literature as those are not related to our present domain of discussion.

The literature clarifies that the doping with the A-site enhances ferroelectric and ferromagnetic response. Among all the elements on A-site we preferred Gd for doping as it has high Bohr's magneton (~8.0 μB) and having similar ionic radius to Bi which may give better stability to perovskite structure and enhance both magnetic and dielectric properties.

Doping at the B-site minimizes the problem associated with leakage current. It is noticed from all the doped elements at B-site aliovalent ions of larger ionic radii reduces the oxygen vacancies as compared to isovalent ions. So, we preferred Mg for substitution in order to enhance magnetic, dielectric properties and improve the leakage current in a stable perovskite structure.

Doping of the ABO_3 system refines both the dielectric and magnetic properties of the pure BFO system. Among all systems doping BZT was preferred as it shows very interesting dielectric properties below MPB.

All three approaches are considered separately with the BSFO system for developing a material having enhanced magneto-dielectric response along with a minimum level of leakage current.

2.8 Objectives of the work

The objective of the present work is to synthesize and characterize doped BFO ceramics with improved multiferroic properties. The investigation comprises of the following stages: (I) the Sm content will be fixed at 0.1, *i.e.*, $(Bi_{0.9}Sm_{0.1})FeO_3$ (BSFO) system and (ii) the BSFO ceramics will be synthesized by the solid-state method. The influence of dopants on the multiferroic properties of the BSFO will be studied with the following objectives:

a) Study the effect of Gd^{3+} doping for Bi^{3+} on the multiferroic properties of BSFO system.

b) Analyse the effect of Mg^{2+} doping for Fe^{+3} on the multiferroic properties of BSFO system.

c) Study the influence of BSFO and BZTO ceramics on the multiferroic properties of BSFO system.